IJCRT.ORG ISSN : 2320-2882

INTERNATIONAL JOURNAL OF CREATIVE RESEARCH THOUGHTS (IJCRT)

An International Open Access, Peer-reviewed, Refereed Journal

INFLUENCE OF PROCESSING PARAMETERS FOR FORMING COBALT BASED MULTI-COMPONENT ALLOY POWDERS

Yogesh Srivastava[1]* and Lav kush[2]

[1]Technology Development Center, Training Division, Ministry of MSME (Formerly Process & Product Development Center), Agra, 282006, U.P., India

[2]Department of Material Science & Metallurgical Engineering, Ceramic & Powder Metallurgy Laboratory Maulana Azad National Institute of Technology, Bhopal, Madhya Pradesh, India (462003)

Abstract

The speed effect in high-energy ball milling with lattice strain induced, milling intensity and dislocation density in mechanically alloyed powder particles as processing parameters. The milling conditions in cobalt-based multi-component powders and their geometry played an important role. The collision geometry inside the vial would lead to fragmentation and coalescence. The mathematical kinematics and dynamics modeling was preferred to find processing conditions, microstructure and reaction mechanism. The structural and morphological properties of milled powders were considered by using sophisticated techniques like Scanning Electron Microscopy (SEM), Transmission Electron Microscopy (TEM) and X-Ray Diffraction (XRD).

Keywords: Mechanical alloying; Kinematics; Dislocation density; Crystallite size; Milling intensity

1. Introduction

Multicomponent alloys are high entropy alloy (HA), forms solid solution with equimolar ratio [1]. According to the Gibb's free energy, ΔS_{mix} measured stabilizes the evolution over intermediate phases [2]. These multicomponent alloys with different atomic radii cause astringent strain with possible ductility in BCC or FCC crystal [3]. The multicomponent high entropy alloys (HEAs) have attracted scientific interest because of their tunable potential in spintronics applications.

According to the literature reported, mechanical alloying (MA) by means of ball milling is flexible amongst several existing methods for synthesis of alloys for non-equilibrium materials [4-7]. Synthesis of HE multicomponent alloys by mechanical alloying (MA) could lead to many advantages followed by repeated fracturing and cold working [8-13]. During mechanical alloying, several attempts have been made to analyze the mechanistic dynamic approach with speed, time and frequency [14-26]. The overall idea related to change Gibbs free energy by altering the size of

material through mechanical alloying. From the MA process, either material changes into the nano-material or contains maximum glassy phase. Moreover, in nanocrystalline materials, the most important role would be played by surface area and its associated gain boundary surface energy by unit area (γ_{gb}) which can expressed by the following equation:

$$\Delta G_{gb} = \frac{1.5\gamma_{gb}V_m}{r} \quad (1)$$

While free energy to convert crystalline in glassy phase given by:

$$\Delta G_{ls} = \Delta H_{ls}\frac{(T_m - T)}{T} \quad (2)$$

Where, ΔH_{ls} is enthalpy of melting at melting temperature T_m, and molar volume V_m. The theoretical radii for glassy phase from transformation process in nanocrystalline material is responsible for slip propagation from grain to grain and is expressed by:

$$r_c < 1.5\frac{\gamma_{gb}V_m}{\Delta G_{ls}}$$

This is because of stress concentrations formed at dislocation pileups. As a results of stress concentration between dislocation, applied stress can split two edges dislocation at a minimum separation distance l_c; given by:

$$l_c = \frac{Gb}{\pi(1-\upsilon)\sigma_a}$$

where, G, b and υ respectively are shear modulus, Burgers' vectors and Poisson ratio [27].

Maurice et al. [14, 15] explained the strain rate, dynamic impact, rise in temperature during milling and cooling rate used in milling kinetics using Hertzian criterion. Subsequently, Burgio et al. [16] studied the equations to calculate the acceleration and speed of grinding media which is used in computing energy the transferred to powder particles. Abdellaoui and Gaffet et al. [17-19] analyzed the ball impact power rather than frequency and kinetic energy. Watanabe et al. [24] also discussed ball trajectory and kinematics using Kelvin's mechanical model. However, Dallimore and McCormick explained about the motion of grinding medium using elemental model [25]. Earlier investigations conducted until now explored milling parameters and its influence in finding kinetics of alloying. Present wok investigates the detailed study of milling parameters of cobalt based multicomponent alloy powders prepared by mechanical alloying.

2. Materials and Experimental procedure

Commercially available elemental powders of Cobalt (99.9 % purity), Chromium (99.9 % purity), Aluminum (99.9 % purity), Manganese (99.9 % purity) and Tin (99.9 % purity) supplied by Alfa Aesar, USA used as starting material constituents. Before mixing, powders annealed for 30 min. in hydrogen atmosphere to reduce if any surface oxides present in it. The reduced powders mixed in ratio of 60 wt.%, 26 wt.% and 14 wt.%. The composition gained was then allowed for mechanical alloying in high-energy planetary ball mill (Pulverisette-5) supplied by Fritsch GmbH, Germany. During mechanical alloying, tungsten carbide balls (10 mm) used as grinding medium. The milling jars having capacity of 250 ml and internally lined with tungsten carbide. The process was carried out at a variable speed of 100-400 rpm maintaining ball-to-powder ratio (BPR) as 10:1. During the process, wet milling was carried by using excess amount of process control agent (PCA) to avoid contamination and agglomeration in the system. To limit

the process and avoiding the welding between vials and balls, milling was paused periodically at every 20 minutes. The powder samples were collected at various stages of milling for their morphological analysis. The approach used to calculate crystallite size and lattice strain is based on procedure discussed elsewhere [7, 28]. In this approach, three most intense peaks in X-ray Diffraction (XRD) spectra used for calculation. The phase evolution in the milled powder samples was studied by using monochromatic XRD, Pananalytical, X'Pert Pro equipped with copper target. The milled powder samples compacted under single acting hydraulic press in a circular die with an internal diameter of 10 mm. Microstructural characterization and composition of milled powders carried out using Scanning Electron Microscopy (SEM) (JEOL, JSM-6390A, Japan) by accelerating voltage 10 kV and Transmission Electron Microscopy (TEM). Electron Microscopy (EM) used to study the morphological feature and distribution of particle size in powder particles.

2.1 Morphological analysis

The morphological feature and distribution of particle size for MAed powder particles produced after milling was examined by using Scanning Electron Microscopy (SEM) (JEOL, JSM-6390A, Japan) equipped with EDS with accelerating voltage 10 kV and Transmission Electron Microscopy (TEM).

2.2 Structural phase evolution

The structural phase formation and evolution of average grain size information has been revealed from X-ray diffraction using CuK_α radiation by scanning 2θ angle ranging from 30^0 to 90^0 taking step size as 0.02^0 with integration time 4 seconds. The broadening of peaks in X-ray can be explained by Voigt and Gaussian function [29]. The instrumental broadening has been corrected using standard silicon as reference material. By assuming **r** as measured line profile which is considered for standard profile **q** with structurally broadened profile **p**, includes the strain and size effects. For instance, if **p** and **q** considered to be Voigt functions, then

$$r_C = q_C * p_C \text{ and } r_G = q_G * p_G \tag{3}$$

where, C and G of r and q profiles gained from FWHM and peaks internal breadth [30]. Average crystallite size and induced lattice strain estimated by using relation:

$$(\beta_t - \beta_o)\cos\theta = \frac{0.9\lambda}{D} + 4(\varepsilon)(\sin\theta) \tag{4}$$

where, λ is CuK_α radiation wavelength, $(\beta_t - \beta_o)$ is FWHM of milled powders and ε is the lattice strain induced during milling.

3. Mathematical Analysis

3.1 Dynamic of energy calculation

On considering that if the balls do not change the speed along the flight, then the energy input during milling can be expressed as [12]:

$$E_b = \frac{1}{2} m_b V_b^2 \tag{5}$$

and the speed of ball given by the following expression:

$$V_b = \frac{2\pi}{60}\left[R_p{}^2\Omega^2 + \left(R_v - R_b\right)\omega^2\left(1+2\frac{\omega}{\Omega}\right)\right]^{0.5} \tag{6}$$

where, R_p, R_v and R_b will be the radii of plate, vial and the balls respectively, ω and Ω will be angular frequency of plate and vial, m_b, V_b, and N_b is the mass of balls, speed of balls and the number of balls. Total milling intensity I_t (energy each weight unit of powder) is given by:

$$I_t = \frac{\varphi E_b N_b t}{w_p} \tag{7}$$

Where φ is impact frequency , t milling time and w_p is weight of powder. The impact frequency calculated from the following expression :

$$\varphi = \frac{60(\Omega - \omega) n_b}{2\pi} \tag{8}$$

Joardar et.al. [31] explained milling of nanocrystalline NiAl alloy by dynamics and reported the existence of long-range ordered structure under various conditions. They considered planetary motion of balls and formulated the efficiency factor according to equation (8) by incorporating the large number of grinding balls in the vial.

3.2 Milling motion Kinematics

In evaluating balls position on vial surface during alloying in ball mill, we will consider the kinematic of single ball inside the vial [16, 17]. So for to calculate individual impact, amount of energy transferred by balls to powder. It supposed that kinetic energy conserved in colliding bodies. The kinematics of ball rotation clearly described by Abdallaoui and Gaffet et al. [17] as shown in **Figure 1**. According to schematic drawing, consider radial distance of collision and vial as r_d and r_v. The angular rotation of main disc is ωd and that of vial is ω_v. At the early stage of motion i.e. t = 0, P (X_0, Y_0) is the ball position. Similarly, at whatever time t, ball position (x, y) expresses as:

$$x = r_d \cos \omega_d t + r_v \cos (\omega_d - \omega_v) t \tag{9}$$

$$y = r_d \sin \omega_d t + r_v \sin (\omega_d - \omega_v) t \tag{10}$$

Similarly, the speeds in respective x and y directions may be given as:

$$v_x = dx/dt = - \omega_d r_d \sin \omega_d t - (\omega_d - \omega_v) r_v \sin (\omega_d - \omega_v) t \tag{11}$$

$$v_y = dy/dt = \omega_d r_d \cos \omega_d t - (\omega_d - \omega_v) r_v \cos (\omega_d - \omega_v) t \tag{12}$$

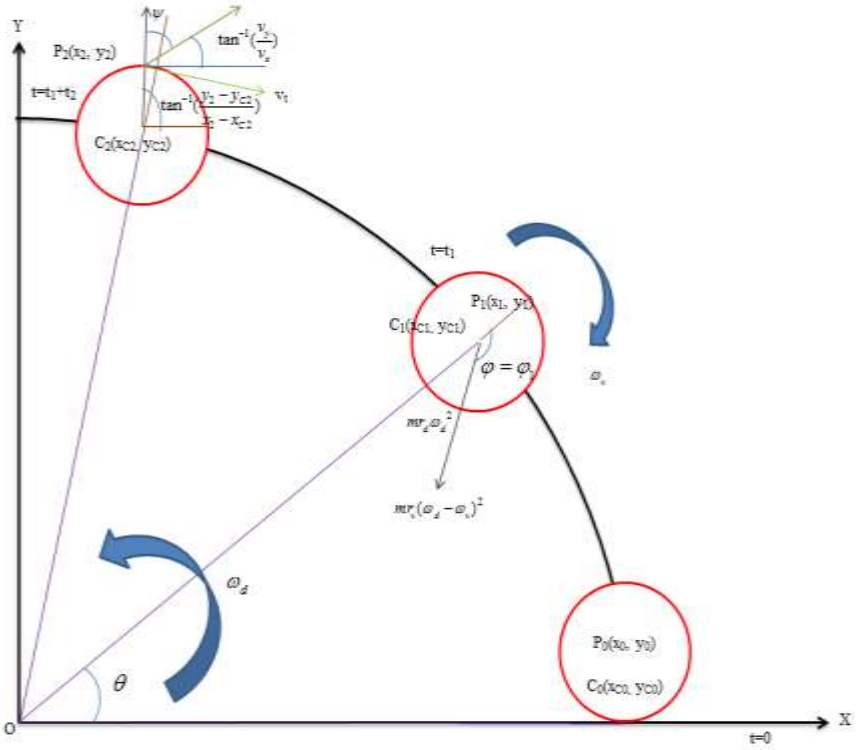

Figure 1 Schematic diagram illustrating the ball position on vials surface [17-19]

4. Results and Discussion

4.1 Microstructural Study

The microstructural and morphological variations at different milling intervals is shown in **Figure 2-4**. At early stage of milling, powder particles deformed by compression forces representing the characteristic of ductile to ductile transition. In general, the exponential relation is valid between the deformations. The crystallite size is given by :

$$k = 30\exp(-1.03\varepsilon) \qquad (13)$$

where, ε is strain produced in material.

By using this expression, Maurice et al. [14,15] analyzed the thickness of lamellae structure and suggests it's exponential relation from deformation of material during mechanical alloying process.

The SEM results reveals the presence of two kinds of phases ie., the phase with spherical morphology and other with flaky. During milling, the constituents with brittle nature converted into angular or sub angular or spherical nature. While the ductile phases had resulted in flaky morphology. The size of flakes/ angular particles were decreasing with milling time. Finally, MAed powder particles found to be about 10 nm particles of brittle phase. Moreover, certain form of agglomeration in the milled particles can be clearly seen at a rotational speed of 150 rpm during milling. This agglomeration is because of predominance of welding mechanism and increased inter-diffusion of Al, Cr, Mn and Sn in Cobalt. After certain hours, a steady state condition arises where an equilibrium exists between the rate of welding and fracturing [32, 33]. As milling continued after this condition, smaller particles undergo to bear more deformation. Agglomerate creating the larger particles without any further decrease in size.

The deformation occurs between powder particles because of the stacking fault energy which results in the slip dislocation and dominates it. It is reported that dislocation slip in nanostructured material obstructed by small sized grains which effects to continue the twinning. Homogeneous nucleation inside grain boundaries overlap stacking faults of dissociate dislocations.

The associated phenomenon at different milling intensity shown in **Table 1**. From tabulated results, it was clearly understood that the use of 10mm balls can increase milling intensity. Furthermore, as milling proceeds, re-welding of particles increases fracturing intensity which improves homogeneity and particles morphology. As we observed, the morphology between 100 rpm and 250 rpm milling speed shows coarser particles but almost perfect homogeneity occurs after prolonged hours. The results obtained shows better efficiency in accordance with results achieved from greater kinetic energy of balls which is sufficient enough to rupture larger elemental particles [1]

In mechanical alloying, the continuous deformation of powder particles is due to severe plastic deformation of cobalt, chromium, manganese, tin and aluminum particles. Maurice and Courtney [14] taking logarithm of ratio between the original and actual thickness of particle and calculated the strain developed in MAed powder. In the early stage, welding between the particles formed during collision. As the deformation increases, the phase shift will occur by self-propagation of induced temperature. On interesting note, it was found that the crystallite size reaches a minimum and rms strain reaches a minimum value, possibly because of stress relaxation. TEM study confirmed that the value of crystallite size obtained is in good agreement with values estimated from XRD data. **Figure 5-7** shows TEM micrographs for Co_2CrAl, Co_2MnAl and Co_2MnSn MAed powder particles. Also increased lattice constant with increasing milling speed implies that aluminum and tin dissolved into cobalt lattice forming solid solution [34].

Table 1 Milling condition and calculated parameters for preparation of alloy after 50 hr

S.No.	(ω_v)	($\Omega_p=\omega_v/2$)	BPR	Time (hrs)	Ball (mm)	PCA	Velocity (m/sec)	E_b (Joule)	Milling Intensity, I_t (J/g) x10^3
1	100	50	10:1	50	10	Stearic acid	0.6394	0.0016	0.0363
2	150	75	10:1	50	10	Stearic acid	0.9591	0.0036	0.818
3	200	100	10:1	50	10	Stearic acid	1.2787	0.0064	1.4544
4	250	125	10:1	50	10	Stearic acid	1.5984	0.0100	2.2725
5	300	150	10:1	50	10	Stearic acid	1.9181	0.0145	3.2725
6	350	175	10:1	50	10	Stearic acid	2.2378	0.197	4.4542
7	400	200	10:1	50	10	Stearic acid	2.5575	0.0257	5.8177

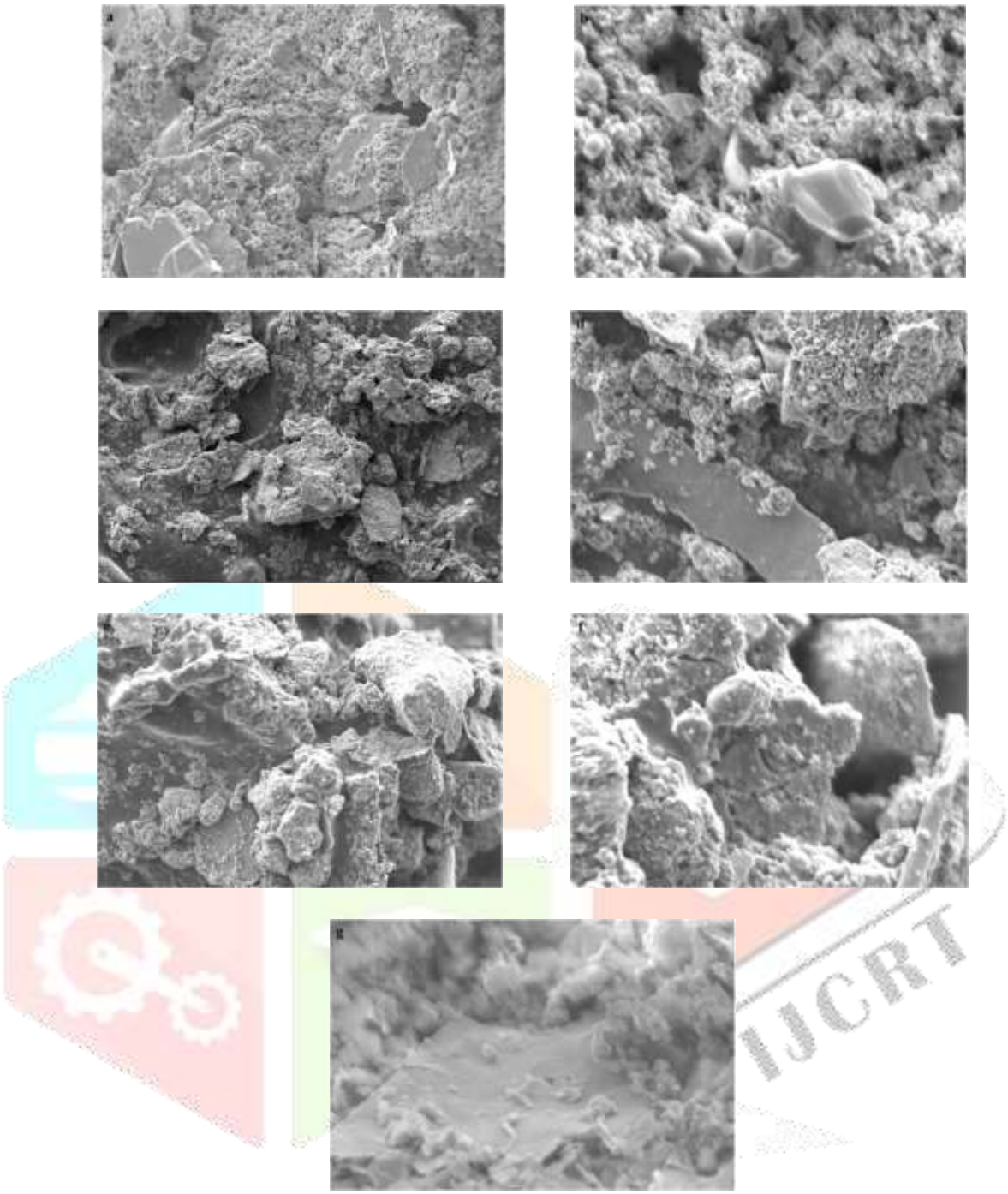

Figure 2 SEM micrograph of Milled Co_2CrAl powder at various speed (a) 100 rpm (b) 150 rpm (c) 200 rpm (d) 250 rpm (e) 300 rpm (f) 350 rpm (g) 400 rpm

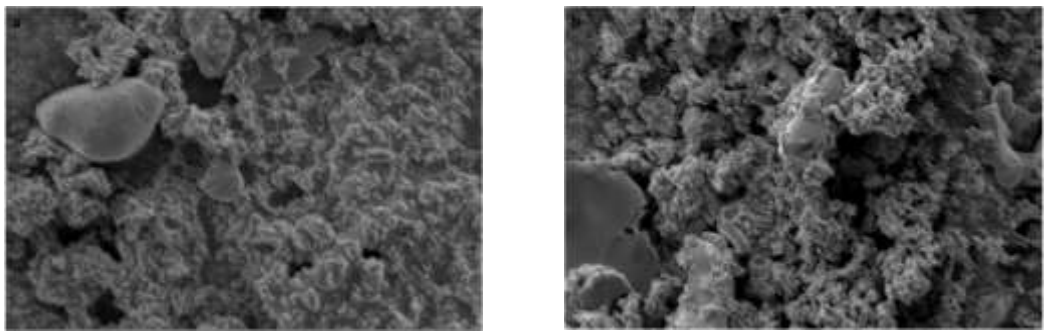

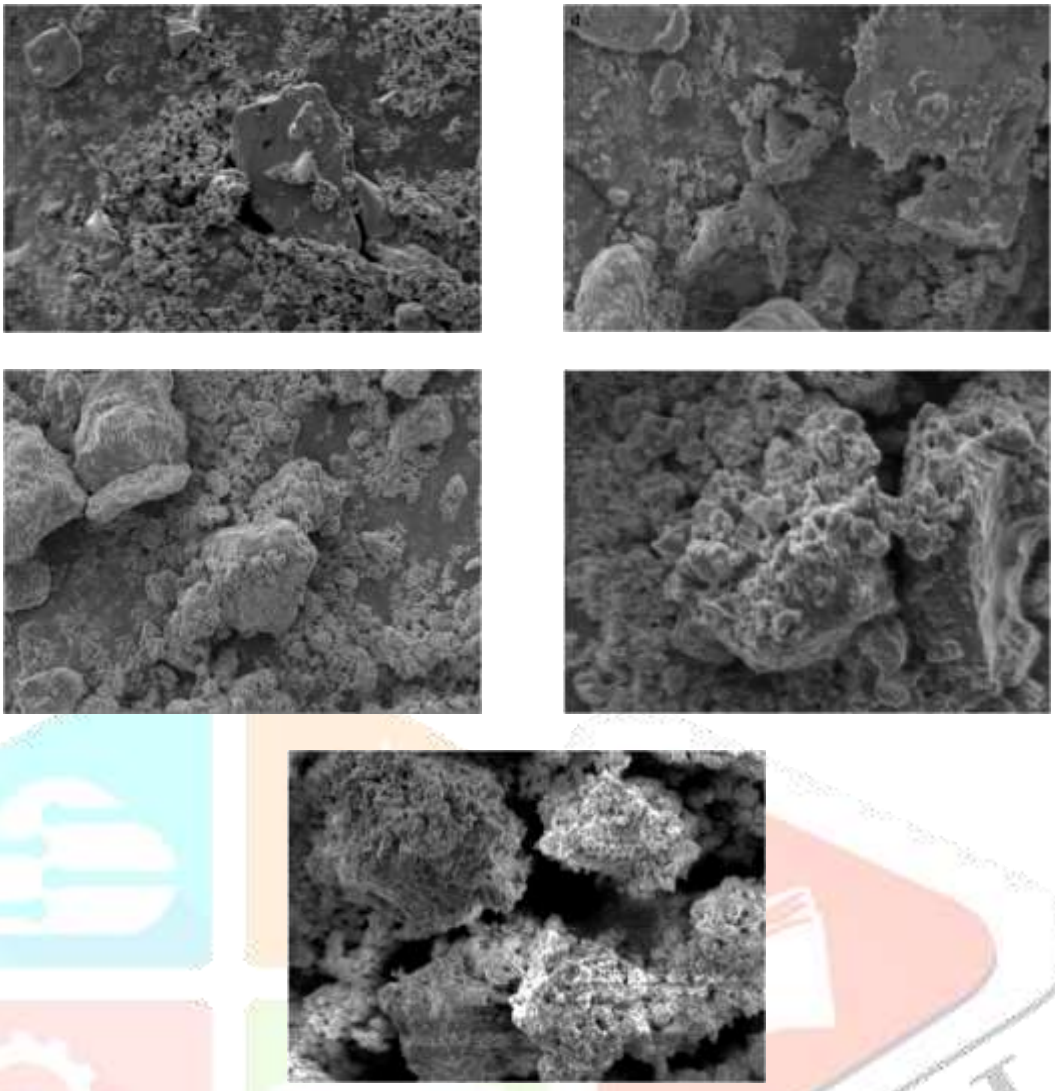

Figure 3 SEM micrograph of Milled Co_2MnAl powder at various speed (a) 100 rpm (b) 150 rpm (c) 200 rpm (d) 250 rpm (e) 300 rpm (f) 350 rpm (g) 400 rpm

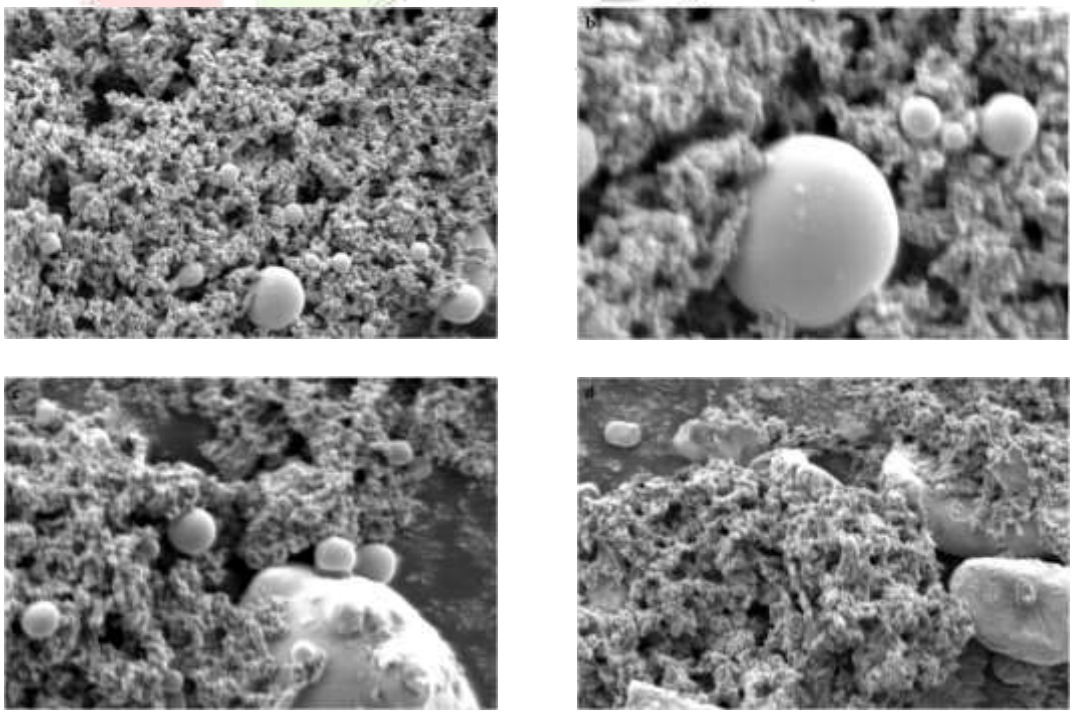

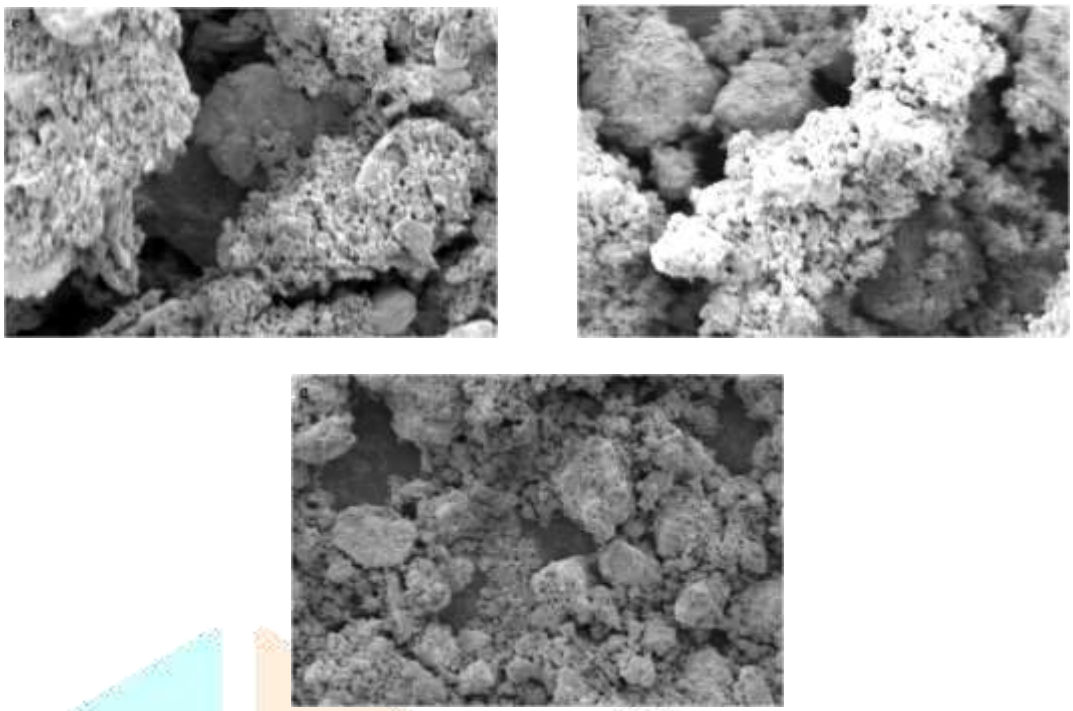

Figure 4 SEM micrograph of Milled Co_2MnSn powder at various speed (a) 100 rpm (b) 150 rpm (c) 200 rpm (d) 250 rpm (e) 300 rpm (f) 350 rpm (g) 400 rpm

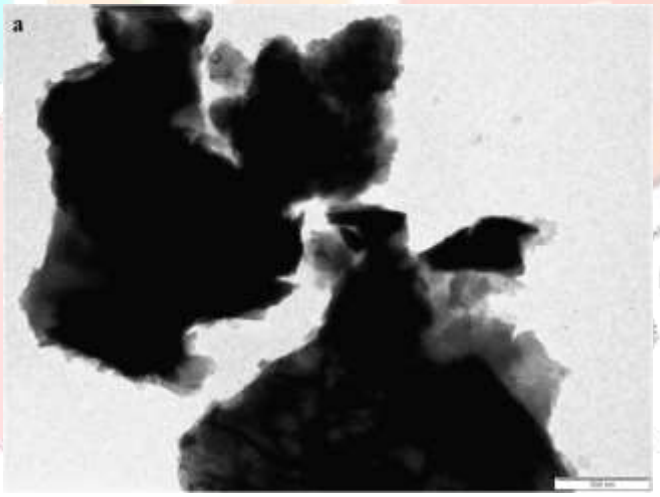

Figure 5 TEM micrograph of Co_2CrAl at 400 rpm

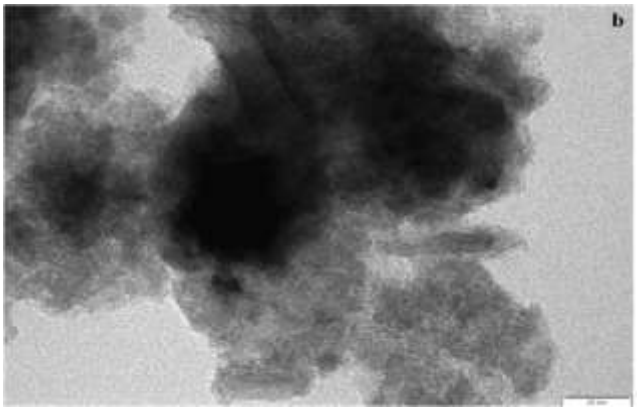

Figure 6 TEM micrograph of Co_2MnAl at 400 rpm

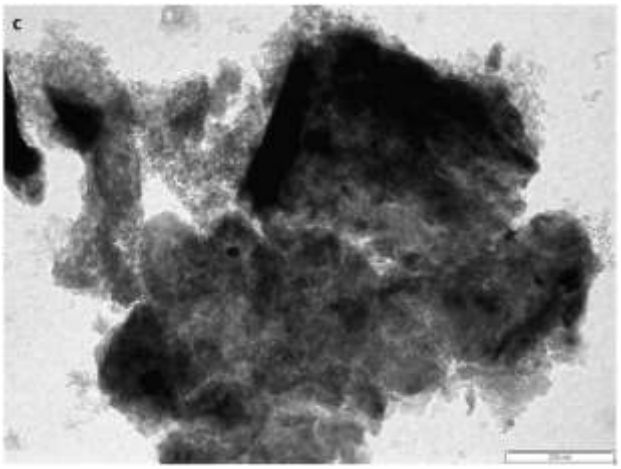

Figure 7 TEM micrograph of Co_2MnSn at 400 rpm

4.2 STRUCTURAL PHASE ANALYSIS

Figure 8-10 shows the XRD pattern of Co_2CrAl, Co_2MnAl and Co_2MnSn powders at different milling times and variable speeds. No oxide peaks are visible in the XRD profile because of the continuous use of PCA. According to XRD profiles, there shows an increase in peaks broadening with the increase in milling period, which result in the lattice strain development and grain refinement as well. Another noticeable fact from XRD pattern, shifting of peak towards the lower angle. The evolution of average crystallite size (L), and the strain (σ) of powders mixture is shown in **Figure 11**. It shows noticeable rapid decrease in crystallite size in 100 to 300 milling speed followed by a sluggish decrease from 300-400 rpm values. Average crystallite size of mixture powder nearly found to be 14 nm. In the early stage, Al peak dissolved at 150 rpm speed forming solid solution. During the various stages, it is noticeable that owing to severe distortions introduced in lattice that would lead to severe plastic deformation during mechanical alloying of powder particles. As the milling speed exceeds, the crystalline phase varied accordingly.

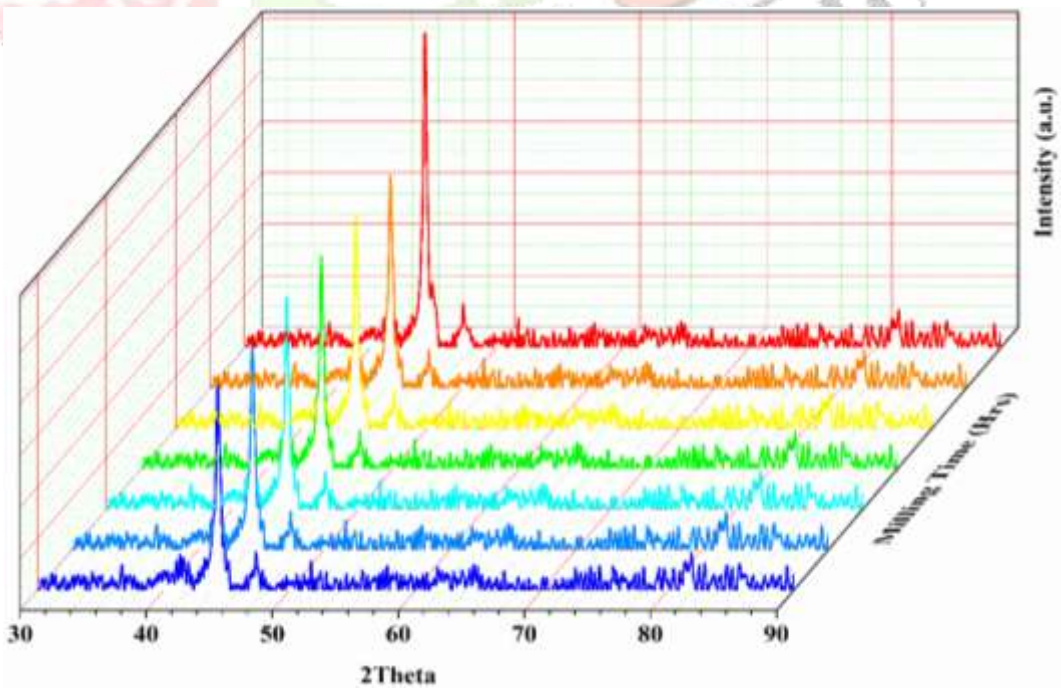

Figure 8 XRD profile spectra of Co_2CrAl at variable speeds

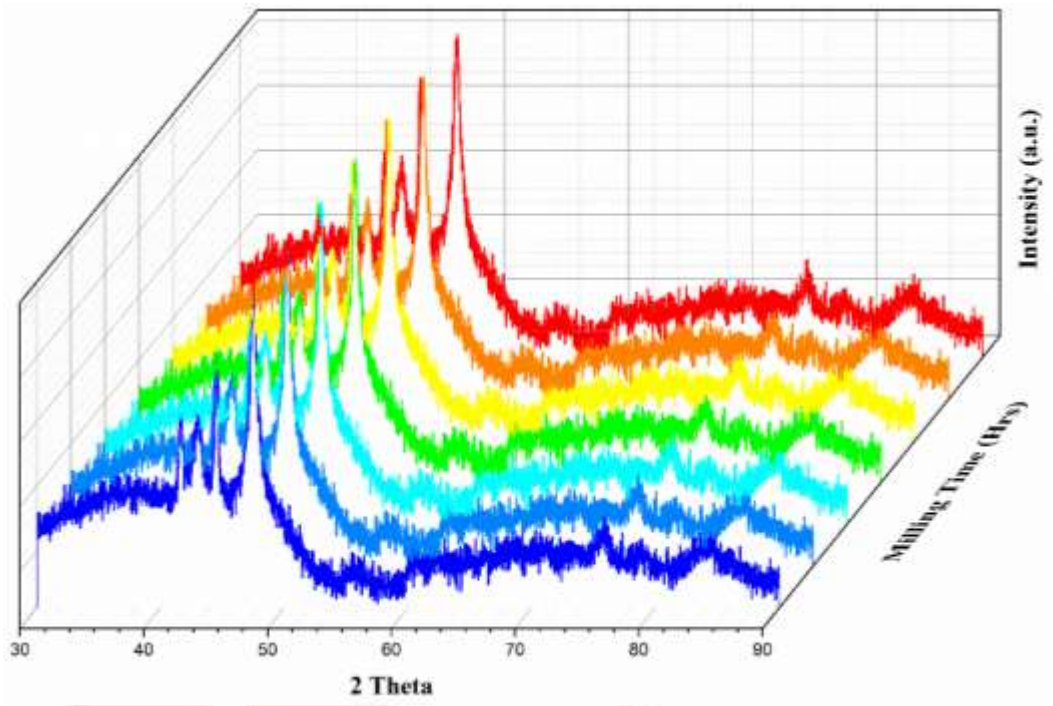

Figure 9 XRD profile spectra of Co_2MnAl at variable speeds

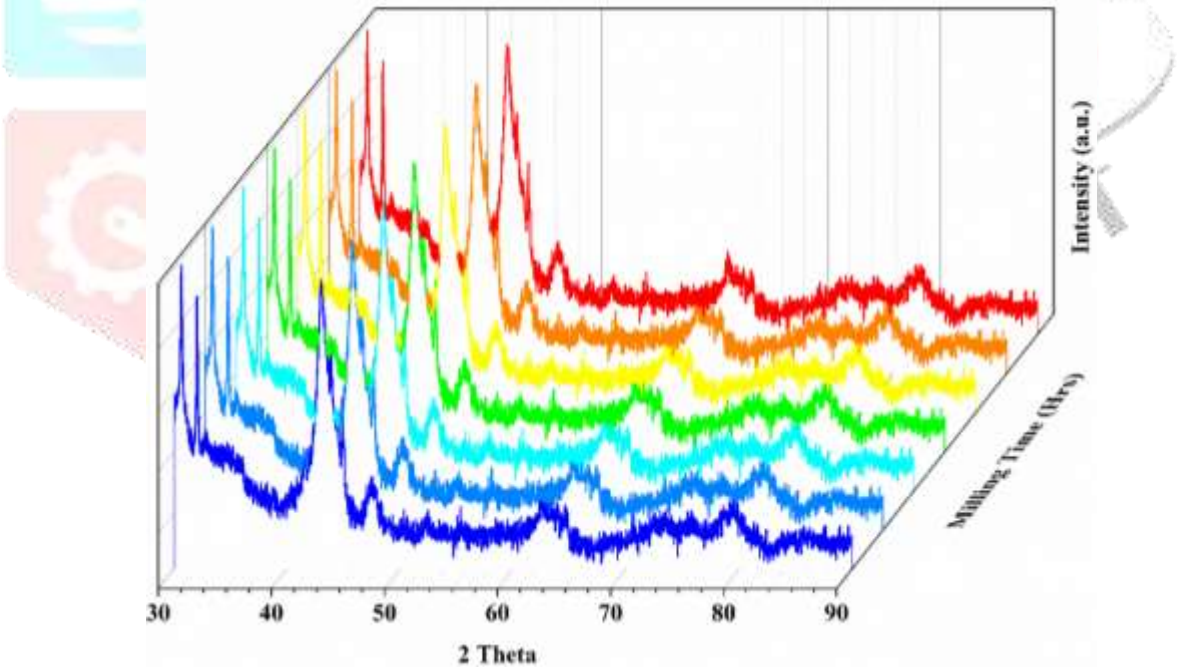

Figure 10 XRD profile spectra of Co_2MnSn at variable speeds

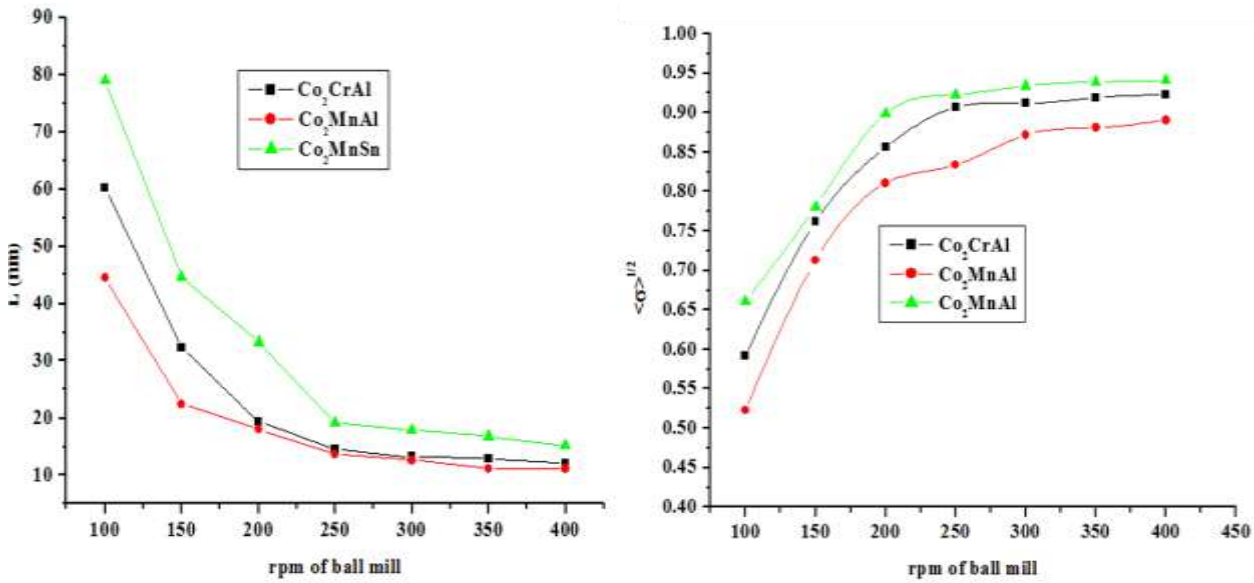

Figure 11 Variation in crystallite size and micro-strain in Co_2CrAl, Co_2MnAl and Co_2MnSn with different rpm values

After 250 rpm of milling speed, peaks start to merge which results in their intensity decrement. The decrease in peak intensity increases milling intensity with speed of the milling (as shown in **Figure 12)**. However, the energy between atoms cause temperature increases as milling intensity increases which results to decrease the diffusion coefficient [35]. Another noticeable interesting point, calculated milling intensities are close with broader peaks suggesting comparably smaller crystallite sizes and overall much better alloying in 400 rpm was realized.

Figure 13 explains the percentage of phase evolution during milling. The phase formation noticed within 30 hours of mechanical alloying at 200 rpm. This milling time led to disappearance of Al peaks. Crystalline refinement and atomic scattering of aluminum to a few nanometers results in broadening of XRD peaks. The lattice constant also shows a variation of milling as shown **Figure 14**. In milling, lattice constant continuously increases up to maximum value of 1.76 nm roughly. The increase in lattice parameter described because of introduction of internal strains through severe plastic deformation or diffusion of Al, Cr, Mn and Sn in Co lattice [36]. The crystallite size and dislocation density results shows fracturing of particles which gets dominated till 30 hours. However on subsequent milling, the dislocation density predominates showing the constituents are elastic in nature.

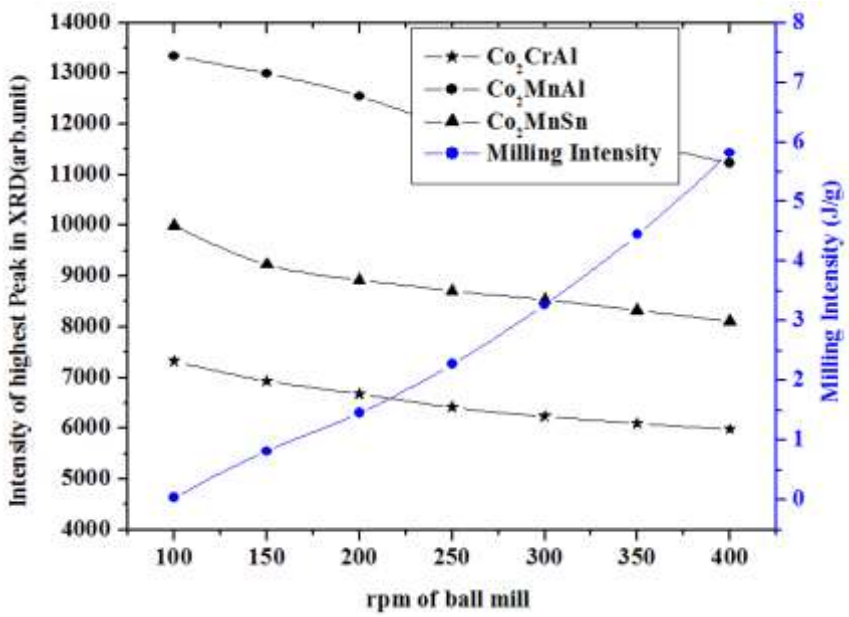

Figure 12 Variation of peak intensity and Milling intensity at various rpm

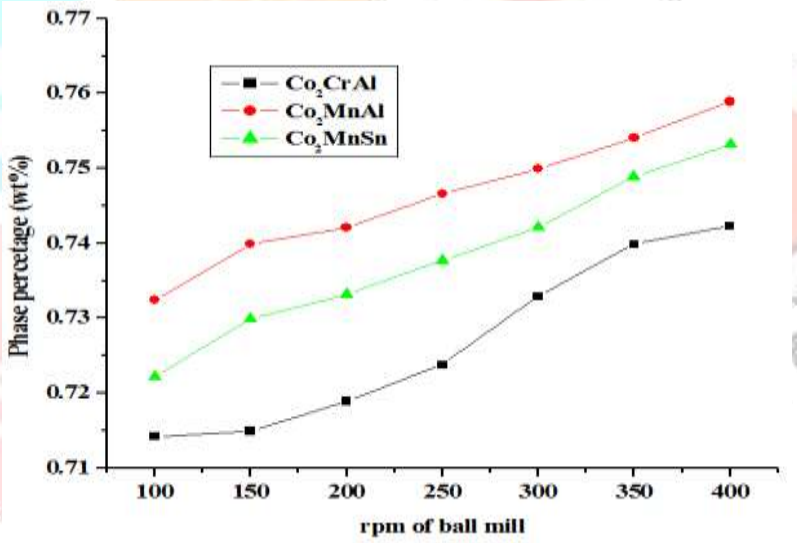

Figure 13 Variation of phase percentage in Co_2CrAl, Co_2MnAl and Co_2MnSn with different rpm values

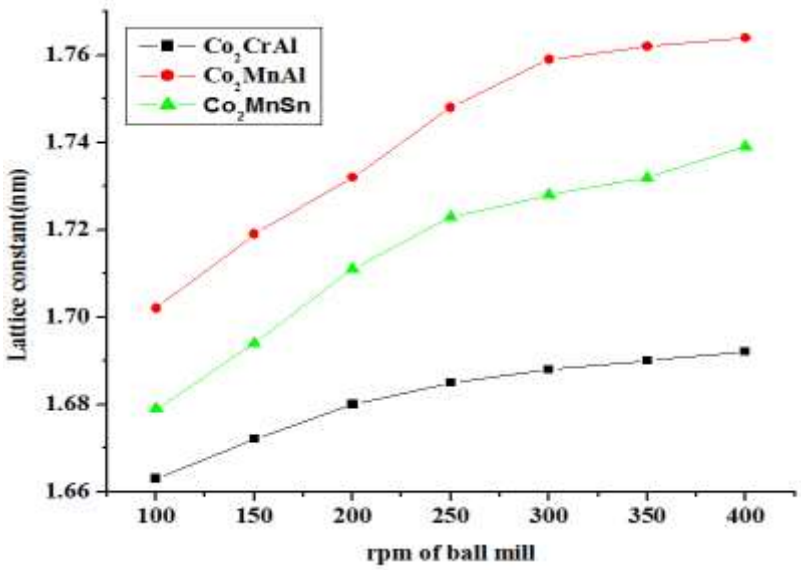

Figure 14 Change of lattice constant in Co_2CrAl, Co_2MnAl and Co_2MnSn

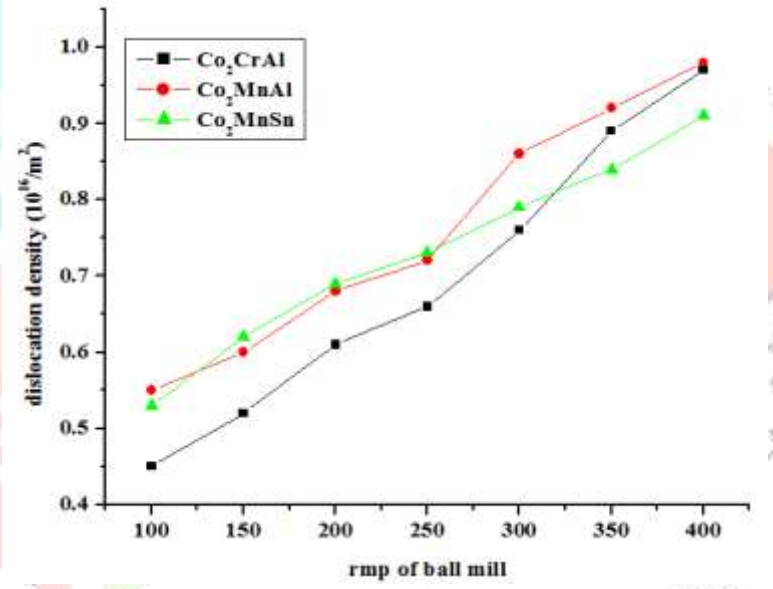

Figure 15 Change of dislocation density in Co_2CrAl, Co_2MnAl and Co_2MnSn under different milling speeds

Dislocations are often linear defect responsible for plastic deformation in mechanically alloyed materials. The dislocations density represented by following equation [36, 37]:

$$\rho_D = 2\sqrt{3}\frac{(\sigma)^{1/2}}{(L)b} \qquad (14)$$

Where b is Burgers vector of dislocations which is equal to 0.3420 nm for Co; L is crystallite size and σ is micro strain. Two sections of density dislocation clearly noted in **Figure 15**. While milling, usage of 100 rpm to 250 rpm, dislocation density slightly increases from $0.45*10^{16}/m^2$ to about $0.63*10^{16}/m^2$. The dislocation density shows a considerable increase and reaches a maximum value of about $0.97*10^{16}/m^2$ in 300 rpm and 400 rpm. This can be explained by the fact that during the milling, collision takes place between balls that gave rise to temperature, so the

dislocations may undergo climb. Owing to this, dislocation formed may undergo by moving no conservatively out of their glide plane with atomic defects which needs greater energy. So diffusivity increased by decline of crystallite size. Also, instance of plastic deformation will induce a local fusion. It supports alloy formation by diffusion at high temperatures. The diffused layers within powder particle continuously fractured lead in diminishing diffusion distance.

5. Conclusions

Co-based multicomponent alloy powders successfully prepared by mechanical alloying. From earlier results reported, it infers that milling conditions played a necessary role and would be a responsible factor in getting desired properties. For carrying out desired properties namely crystallite size, particle size homogeneity in material, milling carried out for 50 hours at variable speeds ranging from 100 rpm to 400 rpm. In doing so, continuous use of process control agent is important to avoid the welding mechanism. Based on experiment performed, the material loses its crystalline nature either on milling beyond 50 hours or on increasing the speed. Both factors are responsible for development of amorphous nature in alloyed powder.

References

[1] I. MORAVČÍK, J. ČÍŽEK, I. DLOUHÝ, MULTICOMPONENT ALLOY POWDERS PREPARATION BY MECHANICAL ALLOYING.
[2] J.W. Yeh, S.K. Chen, S.J. Lin, J.Y. Gan, T.S. Chin, T.T. Shun, C.H. Tsau, S.Y. Chang, Nanostructured High-Entropy Alloys with Multiple Principal Elements: Novel Alloy Design Concepts and Outcomes, Advanced Engineering Materials, 6 (2004) 299-303.
[3] Y. Zhang, T.T. Zuo, Z. Tang, M.C. Gao, K.A. Dahmen, P.K. Liaw, Z.P. Lu, Microstructures and properties of high-entropy alloys, Progress in Materials Science, 61 (2014) 1-93.
[4] H. Gleiter, Nanocrystalline materials, Springer1991.
[5] E. Hellstern, H.J. Fecht, Z. Fu, W. Johnson, Structural and thermodynamic properties of heavily mechanically deformed Ru and AlRu, Journal of applied physics, 65 (1989) 305-310.
[6] B. Murty, S. Ranganathan, Novel materials synthesis by mechanical alloying/milling, International materials reviews, 43 (1998) 101-141.
[7] C. Suryanarayana, Mechanical alloying and milling, Progress in materials science, 46 (2001) 1-184.
[8] C.S. Babu, N. Koundinya, K. Sivaprasad, J.A. Szpunar, Thermal Analysis and Nanoindentaion Studies on Nanocrystalline AlCrNiFeZn High Entropy Alloy, Procedia Materials Science, 6 (2014) 641-647.
[9] O. Senkov, G. Wilks, J. Scott, D. Miracle, Mechanical properties of Nb 25 Mo 25 Ta 25 W 25 and V 20 Nb 20 Mo 20 Ta 20 W 20 refractory high entropy alloys, Intermetallics, 19 (2011) 698-706.
[10] Z. Tang, M.C. Gao, H. Diao, T. Yang, J. Liu, T. Zuo, Y. Zhang, Z. Lu, Y. Cheng, Y. Zhang, Aluminum alloying effects on lattice types, microstructures, and mechanical behavior of high-entropy alloys systems, Jom, 65 (2013) 1848-1858.
[11] Y. Wang, S. Ma, X. Chen, J. Shi, Y. Zhang, J. Qiao, Optimizing mechanical properties of AlCoCrFeNiTi x high-entropy alloys by tailoring microstructures, Acta Metallurgica Sinica (English Letters), 26 (2013) 277-284.
[12] Z. Fu, W. Chen, S. Fang, X. Li, Effect of Cr addition on the alloying behavior, microstructure and mechanical properties of twinned CoFeNiAl 0.5 Ti 0.5 alloy, Materials Science and Engineering: A, 597 (2014) 204-211.
[13] C. Suryanarayana, Nanocrystalline materials, International Materials Reviews, 40 (1995) 41-64.
[14] D.R. Maurice, T. Courtney, The physics of mechanical alloying: a first report, Metallurgical Transactions A, 21 (1990) 289-303.
[15] T. Courtney, Process modeling of mechanical alloying (overview), Materials Transactions, JIM, 36 (1995) 110-122.
[16] N. Burgio, A. Iasonna, M. Magini, S. Martelli, F. Padella, Mechanical alloying of the Fe− Zr system. Correlation between input energy and end products, Il nuovo cimento D, 13 (1991) 459-476.

[17] M. Abdellaoui, E. Gaffet, X-Ray Diffraction and Mössbauer Studies of Mechanically Alloyed Fe–Ni Nanostructured Powders, Acta Met. Mater, 44 (1995) 1087.
[18] E. Gaffet, C. Louison, M. Harmelin, F. Faudot, Metastable phase transformations induced by ball-milling in the Cu-W system, Materials Science and Engineering: A, 134 (1991) 1380-1384.
[19] E. Gaffet, M. Abdellaoui, N. Malhouroux-Gaffet, Formation of nanostructural materials induced by mechanical processings (overview), Materials Transactions, JIM, 36 (1995) 198-209.
[20] D. Basset, P. Matteazzi, F. Miani, Measuring the impact velocities of balls in high energy mills, Materials Science and Engineering: A, 174 (1994) 71-74.
[21] M. Magini, A. Iasonna, Energy transfer in mechanical alloying (overview), Materials Transactions, JIM, 36 (1995) 123-133.
[22] A. Iasonna, M. Magini, Power measurements during mechanical milling. An experimental way to investigate the energy transfer phenomena, Acta materialia, 44 (1996) 1109-1117.
[23] M. Magini, C. Colella, A. Iasonna, F. Padella, Power measurements during mechanical milling—II. The case of "single path cumulative" solid state reaction, Acta materialia, 46 (1998) 2841-2850.
[24] R. Watanabe, H. Hashimoto, G.G. Lee, Computer simulation of milling ball motion in mechanical alloying (overview), Materials Transactions, JIM, 36 (1995) 102-109.
[25] M. Dallimore, P. McCormick, Dynamics of planetary ball milling: a comparison of computer simulated processing parameters with CuO/Ni displacement reaction milling kinetics, Materials Transactions, JIM, 37 (1996) 1091-1098.
[26] P. Le Brun, L. Froyen, L. Delaey, The modelling of the mechanical alloying process in a planetary ball mill: comparison between theory and in-situ observations, Materials Science and Engineering: A, 161 (1993) 75-82.
[27] A.R. Yavari, Phase transformations in nanocrystalline alloys, Materials Science and Engineering: A, 179 (1994) 20-26.
[28] G. Williamson, W. Hall, X-ray line broadening from filed aluminium and wolfram, Acta metallurgica, 1 (1953) 22-31.
[29] S. Vajpai, B. Mahesh, R. Dube, Studies on the bulk nanocrystalline Ni–Fe–Co alloy prepared by mechanical alloying–sintering–hot rolling route, Journal of Alloys and Compounds, 476 (2009) 311-317.
[30] D. Zhang, Processing of advanced materials using high-energy mechanical milling, Progress in Materials Science, 49 (2004) 537-560.
[31] J. Joardar, S. Pabi, B. Murty, Milling criteria for the synthesis of nanocrystalline NiAl by mechanical alloying, Journal of Alloys and Compounds, 429 (2007) 204-210.
[32] H. Bahrami, P. Kameli, H. Salamati, The structural and magnetic properties of one-step mechanochemical route synthesized La 0.8 Pb 0.2 MnO 3 manganites, Journal of Magnetism and Magnetic Materials, 321 (2009) 2533-2536.
[33] M. Mikami, A. Matsumoto, K. Kobayashi, Synthesis and thermoelectric properties of microstructural Heusler Fe 2 VAl alloy, Journal of Alloys and Compounds, 461 (2008) 423-426.
[34] M. Hansen, K. Anderko, H. Salzberg, Constitution of binary alloys, Journal of the Electrochemical Society, 105 (1958) 260C-261C.
[35] W.-R. Wang, W.-L. Wang, S.-C. Wang, Y.-C. Tsai, C.-H. Lai, J.-W. Yeh, Effects of Al addition on the microstructure and mechanical property of Al x CoCrFeNi high-entropy alloys, Intermetallics, 26 (2012) 44-51.
[36] L. Dekhil, S. Alleg, M. Bououdina, J. Sunol, J. Greneche, Phase transformations and magnetic properties of ball-milled Fe–6P–1.7 C powders, Advanced Powder Technology, 26 (2015) 519-526.
[37] Y. Zhao, H. Sheng, K. Lu, Microstructure evolution and thermal properties in nanocrystalline Fe during mechanical attrition, Acta Materialia, 49 (2001) 365-375.